Design of a Compact Spectrometer for High-Flux MeV Gamma-Ray Beams

Darragh Joseph Corvan* and Gianluca Sarri
School of Mathematics and Physics, The Queen's University of Belfast, BT7 1NN Belfast, UK

Matthew Zepf
School of Mathematics and Physics, The Queen's University of Belfast, BT7 1NN Belfast, UK and
Friedrich-Schiller-Universität Jena, Föstengraben 1, 07740 Jena, Germany
(Dated: March 25, 2014)

A novel design for a compact gamma-ray spectrometer is presented. The proposed system allows for spectroscopy of high-flux multi-MeV gamma-ray beams with MeV energy resolution in a compact design. In its basic configuration, the spectrometer exploits conversion of gamma-rays into electrons via Compton scattering in a low-Z material. The scattered electron population is then spectrally resolved using a magnetic spectrometer. The detector is shown to be effective for gamma-ray energies between 3 and 20MeV. The main properties of the spectrometer are confirmed by Monte-Carlo simulations.

arXiv:1403.5992v1 [physics.ins-det] 24 Mar 2014

I. INTRODUCTION

MeV photons are generated in a wide range of physical scenarios, ranging from unstable nuclei up to massive stellar objects such as pulsars. Effective detection and analysis of the information contained in the photon spectra have resulted in important discoveries in the fields of nuclear physics [1] and astronomy [2], and the development of new sources are important for many applications including security, nuclear physics, and medicine [3–5]]. Accurate and efficient detection of high-energy photons is thus an important area of research for fundamental as well as for applied physics. Currently there are a number of ways of detecting MeV gamma rays, most of which exploiting either Compton scattering or the quantum electromagnetic cascade initiated by the photon in a solid. Compton cameras are compact devices that detect gamma rays by measuring the number of electrons stripped off an atom in the crystal lattice. These free electrons impact onto a scintillator whose photoemission is then collected by a photomultiplier tube and counted. While Compton cameras can give accurate information about flux, they do not give information about the energy of incident photons [6, 7]. On the other hand, the energy of a multi-MeV photon can be measured by detecting the quantum electrodynamic cascade induced during its passage through a material. The size and depth of the cascade yields a direct measurement of the energy of the incident photon [8]. These devices can be extremely accurate but they suffer from the limitation that only single hit events can be precisely resolved. Detectors have been developed which are able to successfully determine the energy of gamma rays as well as their flux simultaneously. These include the EUROBALL cluster [9] which can look at energies up to 10MeV, and more recently the AFRODITE germanium detector array, which can measure gamma rays with energies up to 20MeV [10]. Such detectors track the energy of the gamma by looking at its scattering through a volume of germanium. Information from the scattered electrons can be used to reconstruct the energy of the original gamma-ray. While such detectors are able to perform their tasks with great proficiency, the nature of their tracking means that a large number of germanium arrays are used in the device to build up a picture of flux and that increases the volume they occupy, making their implementation in many laboratories unfeasible. Here we report on a novel design that allows for simultaneous measurements of energy and flux of a multi-MeV gamma-ray beam in a compact detector design. The proposed detector exploits Compton scattering of the gamma-ray photons in a low-Z solid (Li in this case). It is shown that, for a suitable Li thickness, the scattered electron population retains a similar spectral shape as the initial gamma-ray beam, as long as the latter has an energy not exceeding 50 MeV. By measuring flux and spectrum of this electron population by means of a magnetic spectrometer, it is thus possible to deconvolve the signal, retrieving the spectrum of the gamma-ray beam. The main properties of this detector are confirmed by proof of principle experiments [11] and Monte Carlo simulations performed using the code FLUKA [12, 13]. The structure of the article is as follows. Section II will briefly describe the main interaction mechanisms of a multi-MeV gamma-ray beam with a low-Z solid and introduce lithium as the best material for this detection system. Section III will discuss the propagation of secondary particles (photons, electrons, and positrons) after they escape the lithium block and address the signal-to-noise ratio of the detector. The section will also describe the requirements of the magnetic spectrometer for the measurement of the spectrum of the scattered electrons. Finally, in Section IV an overall design of the detector will be presented.

* dcorvan01@qub.ac.uk

II. MEV GAMMA-RAY INTERACTION WITH LITHIUM

Photons may interact with atoms in a number of ways. In the multi-MeV regime, the main interaction mechanisms are photoionization, Compton scattering, and electron-positron pair production. We will hereafter neglect ionization, since the energy loss associated with this mechanism is much smaller than the initial photon energy (≈eV compared to ≈MeV) and focus our attention only on Compton scattering and pair production. Compton scattering between a ≈MeV photon and an electron at rest can be considered to be an essentially elastic process. The forward scattered electron is expected to have an energy comparable to that of the incident photon. On the other hand pair production is most likely to occur in the electromagnetic field of the nucleus. In this case, the process is intrinsically inelastic as momentum can be transferred in a way that allows a large spread of energies (3 body system). In order to generate an electron population with a spectrum similar to the incident gamma-ray beam, we thus need to maximize the probability of Compton scattering if compared to that of pair production. Since pair-production scales with the square of the atomic number Z [14, 15], it is intuitive to expect that an element with low Z would be required. We will thus focus our attention on lithium, which is the material with lowest Z that is solid at standard conditions. Based on the NIST database [16], we can see how Compton scattering is indeed the dominant interaction mechanism for a multi-MeV gamma-ray beam up to energies of 50 MeV (see Fig. 1). Fig. 2 shows that for high energy photons the energy of the Compton electrons is insensitive to the scattering angle over a wide range, forming the basis for the spectrometer design. While the primary

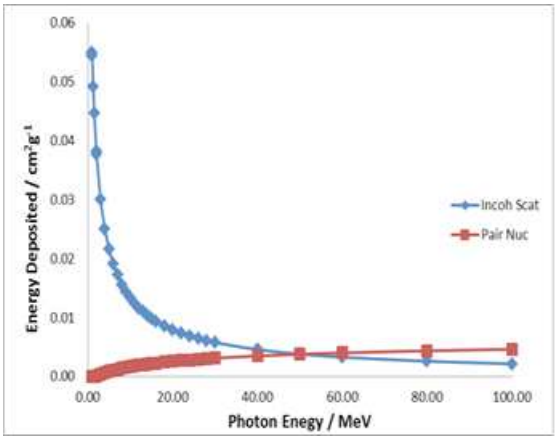

FIG. 1: Energy loss for a multi-MeV gamma ray beam as it interacts with lithium. The red line corresponds to pair production in the nuclear field, whereas the blue line corresponds to Compton scattering. Compton scattering is dominant up to approximately 50 MeV, beyond which pair production dominates. (Data obtained from the NIST database[16]).

Compton scattered electrons are well correlated to the photon energy, good conversion efficiency into Compton electrons necessitates thick lithium converters. In order to determine the effect of the lithium converter on the the spectrum of the electrons escaping the lithium, a series of simulations were performed using the Monte-Carlo code FLUKA. For these simulations we assume pencil-like monoenergetic photon beams of different energy E_γ (1.5, 2, 5, 7, 10, 15, and 20 MeV) incident upon 2cm of lithium. Scattering of the electron in the lithium broadens the electron spectrum and results in low energy tail. This effect can be mitigated by selecting a narrow acceptance angle. This was investigated by simulating 10MeV photons incident on the 2cm lithium and varying the acceptance angle of the electrons detected immediately after it. Equation 1 shows the Compton scattering formula.

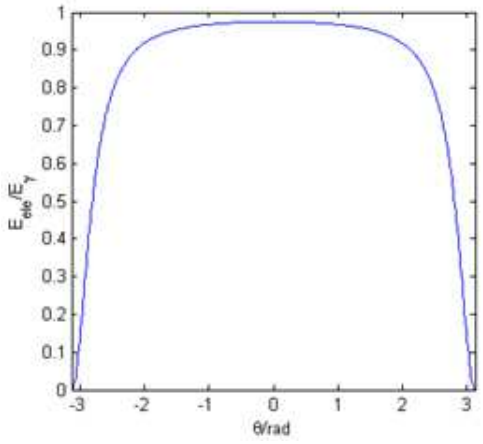

FIG. 2: Angular dependence of the energy of Compton scattered electrons for photon energy of 10MeV. For multi-MeV photons, the electron energy remains largely constant over a large angular range, allowing the energy of the incoming γ-ray to be inferred from the Compton scattered electrons.

$$\Delta\lambda = \frac{h}{cm_e}(1 - cos\theta) \tag{1}$$

Where $\Delta\lambda$ is the change in photon wavelength, h is planks constant, c is the speed of light m_e is mass of the electrons and θ is the angle of the scattered photon. From equation 1 it is trivial to calculate the energy transferred to the electron. From Fig. 3, it is clear that the shape of the peak is maintained for acceptance angles between 2π and 0.2 steradian. However, an angle of 0.2 steradians, the level of the low energy tail significantly reduces. If the acceptance angle is reduced to 0.02 steradians the level of signal decreases rapidly to levels that would be unsuitable for meaningful spectra to be extracted. The focus of attention in the remainder of this paper will be on electrons forward scattered in a narrow cones that give a reasonable compromise between spectral resolution and high signal (0.07 steradian).

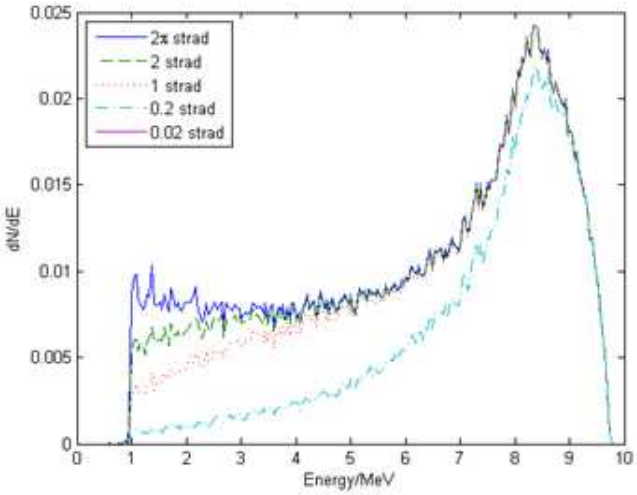

FIG. 3: Spectra of the electrons generated after the propagation of a pencil-like monoenergetic gamma-ray beam of 10MeV through 2cm of lithium for various acceptance angles (see legend). The y-axis corresponds to the number of electrons generated per incident gamma-ray photon per MeV. For the smallest acceptance angle (0.02strad) the yield becomes close to zero.

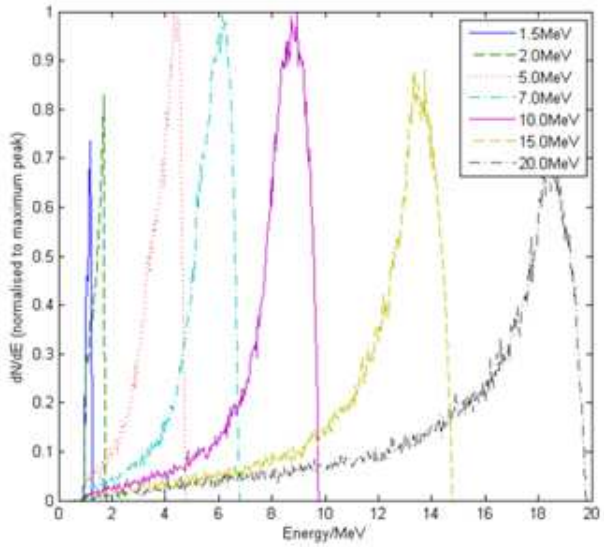

FIG. 4: Spectra of the electrons generated after the propagation of a pencil-like monoenergetic gamma-ray beam through 2cm of lithium (see legend for the different gamma-ray energies simulated). The y-axis corresponds to the number of electrons generated per incident gamma-ray photon per MeV, normalized to the maximum peak. The angle of acceptance for electrons was 70msterad.

Next we consider the dependence of the electron spectra on the incident photon energy. We find a peaked distribution with a maximum at an energy approximately 1.6 MeV less than the incident energy E_i. The full width half maximum increases with increasing photon energy and stabilises at a width of the order of 2 MeV at high energies plus a low energy linear tail for a 2cm thick Li converter. The simulated spectra of this electron population for a range of initial gamma-ray energies are shown in Fig. 4. The spectral broadening and the emergence of the low energy tail is largely due to the scattering of electrons as they move though the material. Thus a trade-off exists between spectral resolution and yield. Fig. 5 shows the effect the various thicknesses of lithium for an interaction with 10MeV photons. The thinner converters achieve a significantly narrower electron peak (< 0.5MeV) at the cost of a noticeable reduction in yield. Note that at lower photon energies the overlap of the response curves limits the achievable resolution and that alternative systems can be used in this energy range. Thus in a high flux environment thin converters combined with deconvolution techniques allow for good energy resolution, while acceptable resolution at high yield can be achieved with thicker converters. The thickness of lithium will largely depend on the flux of photons the user wishes to investigate. With high fluxes, a thinner target can be chosen; for our application a compromise of 2cm was chosen. [17].

The simulations indicate a conversion efficiency into electrons of the order of 1.5 to 3% for a 2cm target, depending on E_i. For a poly-chromatic gamma-ray beam, we thus expect to see a spectrum of the scattered electrons which is a convolution of electron spectra arising from different spectral components in the gamma-ray beam. Fig. 6 shows the peak of the electron spectrum as a function of E_i on a 2cm thick target. The peak position for the 2cm thick target is well approximated in the region of interest by the function;

$$E_p = aE_\gamma + b \tag{2}$$

where E_p is the energy of an electron at the peak of the spectrum and the constant a and b are, respectively: $a = 0.93 \pm 0.01$, $b = (-0.25 \pm 0.01)$ MeV. The number of electrons produced per MeV per incident photon at peak energy is shown as a function of E_γ in Fig. 7. The yield of electrons produced increases as the energy increases up to 5MeV where it begins to plateau before once again decreasing. This is likely due to the electrons having absorbed higher energy and hence being scattered less before the conversion efficiency drops. A Gaussian fit best represents the data:

$$\frac{dN_p}{dE} = C\exp[-\big((E_\gamma - D)\big)^2] \tag{3}$$

where N_p is the peak number of electrons per energy per incident photon in MeV^{-1},$C = 0.016 \pm 0.001\mathrm{MeV}^{-1}$, $D = 9.3 \pm 0.5$MeV and $K = 0.06 \pm 0.001\mathrm{MeV}^{-1}$. It is thus possible to parameterize the expected electron

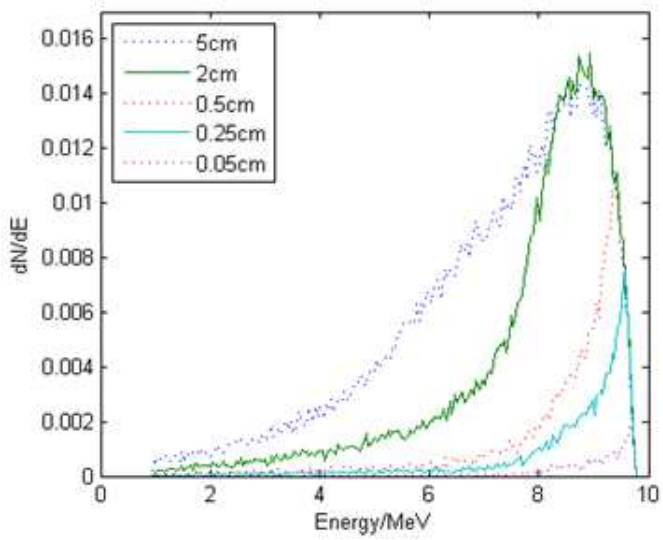

FIG. 5: Spectra of the electrons generated after the propagation of a pencil-like monoenergetic gamma-ray beam of 10MeV through thicknesses of 5cm, 2cm, 0.5cm, 0.25cm and 0.05cm of lithium (see legend for the target thickness simulated). The y-axis corresponds to the number of electrons generated per incident gamma-ray photon per MeV. The angle of acceptance for electrons was 70msterad. As the thickness of the lithium decreases , so too does the FWHM of the peaks. This comes at the cost of reduction to overall yield.

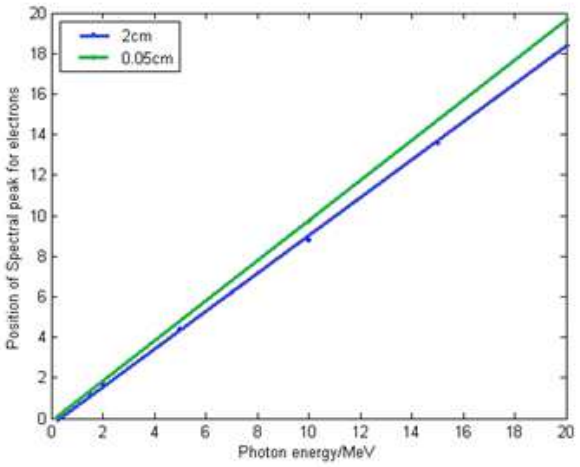

FIG. 6: Fluka simulations show a linear relation between the initial photon energy E_γ and the energy of the electrons escaping the lithium converter. The peak position is affected slightly by scattering in the converter as shown for two converter thickness of 2cm (blue) and 0.05 cm (red).

spectrum in terms of the flux and energy of the incident gamma-ray beam. It thus follows that a deconvolution of

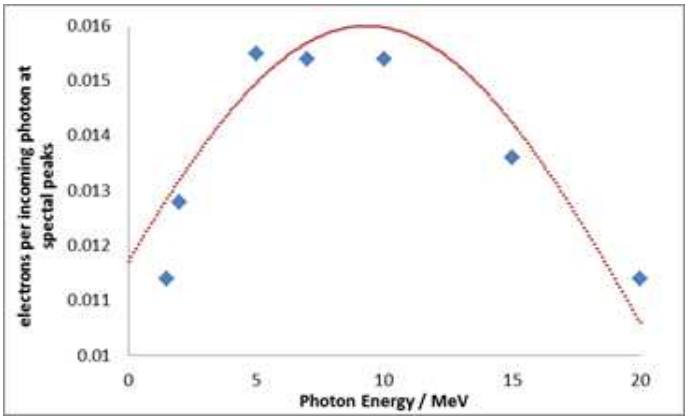

FIG. 7: The peak number of the electron spectra plotted as a function of the initial photon energy. The peaks increase in size up to 5MeV where the peaks remain constant up to 10MeV after which they begin to decrease again. A Gaussian fitting is applied to the trend.

the measured electron spectrum is possible and one can retrieve the spectrum and flux of the incident photons.

As a final remark, it is worth noting that, even if probability of pair production is significantly smaller than that of Compton scattering for $1 < E_\gamma[\mathrm{MeV}] < 20$ (see Fig. 1), neglecting pair production effects introduces a small systematic error in extracting the photon spectrum once the spectrum of the scattered electrons is known. As an example, we plot in Fig. 7 the spectra of the electrons and positrons escaping from the rear surface of the lithium once a pencil-like monoenergetic gamma-ray beam with an energy of 10 MeV is incident upon it. As we can see from Fig. 8, a small population of positrons is indeed generated. Integrating the positron and electron spectrum, we can see that the approximately 12 times more electrons than positrons escape the 2cm thick lithium target. For thinner converter targets (0.5cm and 0.05cm), the low energy tail is almost entirely due to pair production and it is therefore possible to remove it entirely using this technique as long as the flux of incident gammas remains high. FLUKA simulations indicate the spectra of electrons and positrons arising from pair production to be identical, as theoretically expected [14]. The overall electron population will thus consist of the sum of the Compton-driven and pair-production-driven electron spectra. Neglecting pair production effects and assuming all the electrons to arise from Compton scattering will thus induce a systematic error in retrieving the gamma-ray spectrum in the order of 10%. However, a simultaneous measurement of the spectra of the electron and positron populations (see Section IV), allows for subtraction of the latter from the electron spectrum, thus eliminating this source of systematic error.

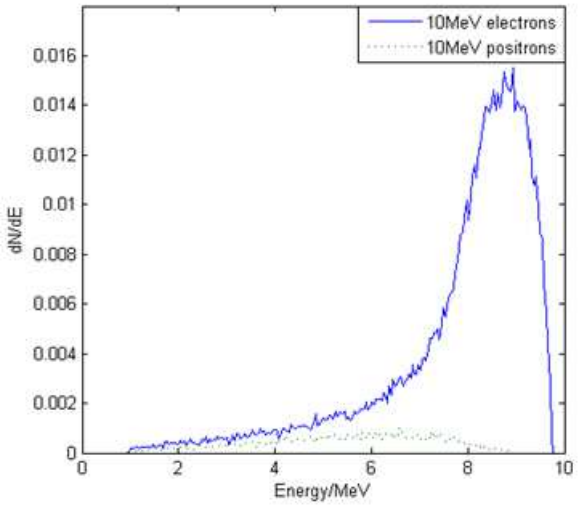

FIG. 8: Spectrum of the electrons and positrons escaping from the rear surface of the lithium block of 2cm thickness once a pencil-like monoenergetic gamma-ray beam with an energy of 10 MeV is incident on it. Results are expressed in number of particles generated per incident gamma-ray photon per MeV.

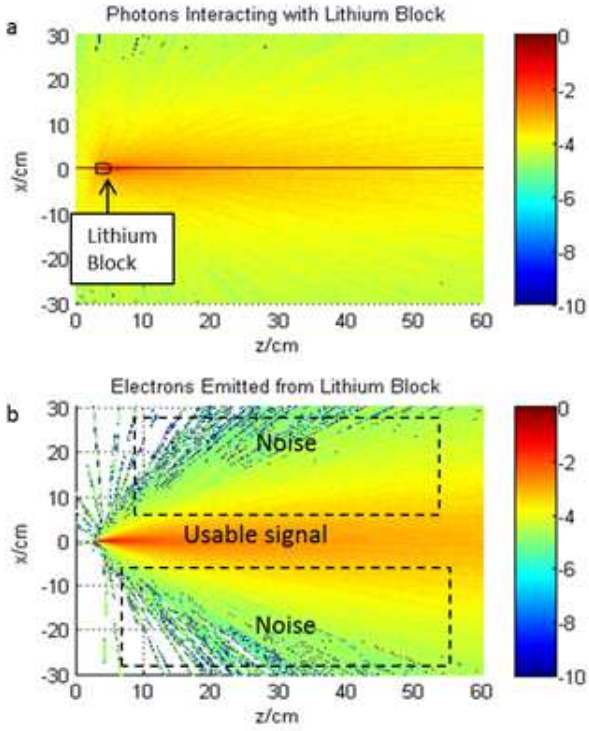

FIG. 9: Spatial distribution of photons (a) and electrons (b) after the interaction of a 10MeV gamma-ray beam with a 2cm thick lithium cube. In both cases, the colourbar represents the number of particles per incident photon per cm (x-axis) expressed as a base 10 logarithm.

III. BEHAVIOUR OF PARTICLES AFTER INTERACTION WITH LITHIUM

In the previous section, we have focused our attention exclusively on the electrons which are emitted on the same axis as the incident gamma-ray beam. This is in principle over-simplifying, since it is well known that Compton scattering present a broad angular distribution. Electrons will thus be emitted also at wider angles, with an energy that gradually decreases as we move far from the axis of the gamma-ray beam. Those electrons thus represent a source of noise for the detector and should be suppressed. Compton scattering will also induce a broadly divergent population of scattered photons, which are again a detrimental source of noise when attempting to measure the spectrum of the scattered electrons. These qualitative arguments are quantitatively corroborated by Fig. 9, which show the spatial photon (9a) and electron (9b) distributions, as resulting from FLUKA simulations, once a pencil-like monoenergetic gamma-ray beam with an energy of 10 MeV interacts with a 2cm thick lithium block. As we can see the vast majority of photons pass through the lithium block without interacting (less than 95% of the initial photons). Also, a population of scattered photons will be isotropically emitted by the lithium (approximately 10^{-3} or 10^{-4} photons per incoming gamma ray photon). The situation is analogous for the scattered electrons. We can see from Fig. 9b that the electron spatial distribution consists of two main parts: a relatively strong population of forward scattered electrons (labelled as usable signal in Fig. 9b) and a wider distribution of electrons scattered widely at both sides of the lithium (labelled as noise in Fig. 9b). This latter population must be suppressed if a good signal-to-noise ratio is to be achieved with the detector. The easiest way to deal with this noise is to introduce a thick lead shielding immediately adjacent to and at either side of the lithium. If we assume a 30cm thick lead wall with an aperture in the middle of the same size as the lithium block, almost all the off-axis scattered electrons and photons are effectively absorbed in the lead. This is shown in Fig. 10 which depicts the simulated photon, electron, and positron spatial distribution for the same initial conditions as the ones used for Fig. 9, with the only difference that a 30 cm lead wall has been now inserted at each side of the lithium block. Whilst, the photon signal on axis has obviously not been affected by this shielding, the off-axis noise has dropped by several orders of magnitude (see Fig. 10). Similarly, the electron distribution off-axis has dropped by the same magnitude. If we now insert a magnetic field at the rear of the lead shielding, we can effectively separate, and spectrally resolve, the electrons and the positrons (see Fig. 10). The spectrally separated electrons and positrons can then be recorded on a suitable,

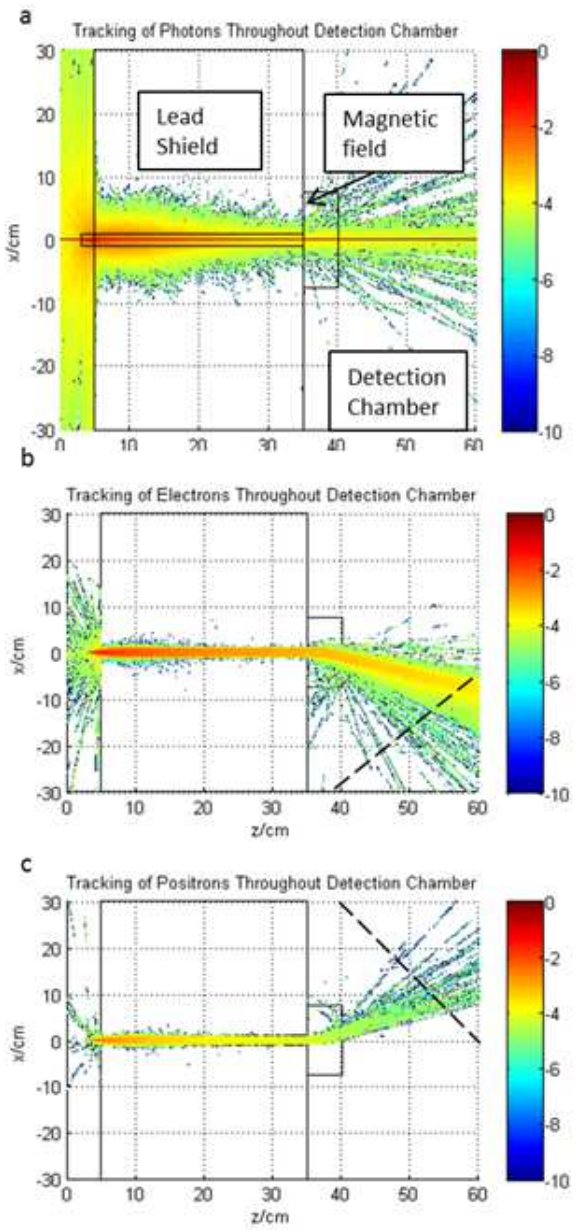

FIG. 10: Spatial distribution of photons (a), electrons (b) and positrons (c) after the interaction of a 10 MeV gamma-ray beam with a 2cm thick lithium cube once the lead shielding and a 5cm-long 0.3T magnetic field is inserted. The colourbar represents the number of particles per incident photon per cm (x-axis) expressed as a base 10 logarithm.

spatially resolved detector, such as an Image Plate or a LANEX screen [18–20]. The spectral resolution of this magnetic spectrometer will depend upon a series of parameters, namely the strength B and spatial extent L_m of the magnetic field, the angular divergence θ_s and source size D_s of the beam, and the distance D_d between the entrance of the magnet and the detector. The relative energy resolution $\delta E/E$ of a magnetic spectrometer in the ultra-relativistic regime ($E \gg 0.5$MeV) thus reads [21]:

$$\frac{\delta E}{E} \approx \frac{E(eV)}{cB(T)} \frac{(D_s + D_d)\theta_s}{(D_d + L_m/2)L_m} \tag{4}$$

Ideally a small aperture, a strong magnetic field, and a long distance between the source and the detector are advisable in order to improve the spectral resolution. However, it is clear that all these parameters significantly decrease the yield of particles on the detector. A trade-off must then be found between a good spectral resolution and a good signal on the detector. Calculations show that a reasonable compromise is found for $B = 0.3$T, $L_m = 5$cm, $\theta_s \approx 30$mrad, $D_s = 1$cm, $D_d = 25$cm (see Fig. 9). As expected, the energy resolution decreases

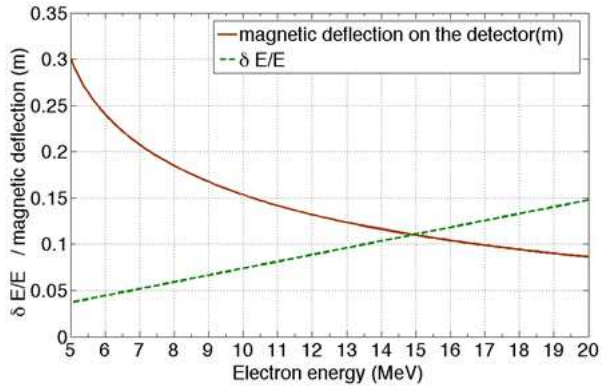

FIG. 11: Relative energy resolution (dashed green line) and spatial deflection on the detector (solid brown line) of the scattered electron population after propagation through a 5cm long, 0.3T magnet. Details in the text.

as the electron energy is increased. However, a relative energy resolution of 4% and 12% are found for 5 MeV and 15 MeV, respectively (energy resolution of 0.2 MeV and 1.8 MeV, respectively). This energy resolution is less than or comparable to the intrinsic energy resolution during the conversion of gamma-ray photons to electrons in the lithium target (see Fig. 11). The resolution of the magnetic spectrometer can also be improved by positioning the detector further away, but at a cost of reduced compactness. As a final remark, it is interesting to note that the vast majority of the gamma-ray photons are able to escape unperturbed from the detector (more than 95%). This allows for simultaneous detection of the spatial profile of the gamma-ray beam, if a suitable detector is placed on axis.

IV. FINAL DESIGN AND CONCLUSIONS

A proposed setup for the detector is depicted in Fig. 12. The gamma ray photon to be measured is incident

upon a 2cm thick lithium block surrounded by 30 cm of lead shielding with a $1\times1\text{cm}^2$ aperture. The entire device shown in Fig. 12, including the shielding is 60cm long and hence, able to fit conveniently into most laboratories. A population of electrons and positrons is generated, the latter arising from pair production in the nuclear field whereas the first generated partially by pair production and mostly by Compton scattering. For a gamma-ray energy window of 1¡E[MeV]¡20, Compton scattering is dominant (see Figs. 1 and 8) allowing for effects due to pair production to be neglected (less than 10% of the overall electron yield). The scattered electrons will have

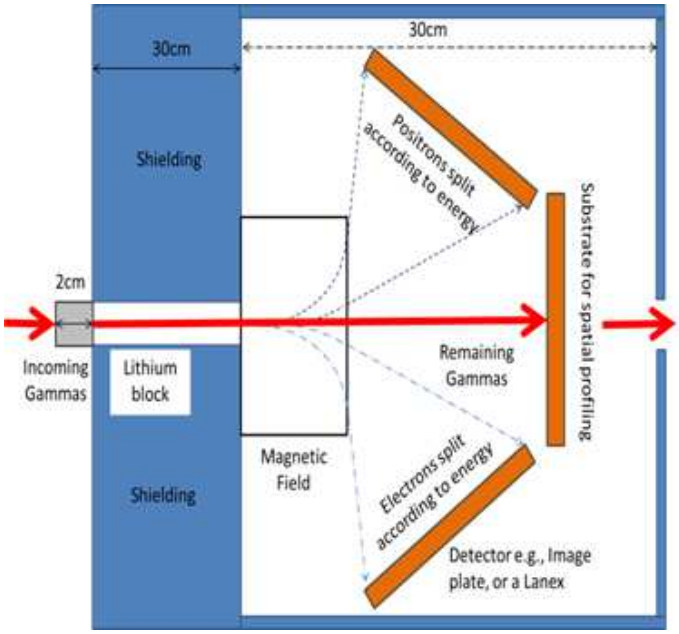

FIG. 12: The proposed setup for the gamma ray spectrometer (not to scale). The entire device is 60cm long in total and consists of 30cm of lead shielding with a 1cm thick gap at the centre before which the Lithium sits. A magnetic field of strength 0.3T is immediately adjacent to this. Image plates can sit off axis in order to detect the charges deflected. On axis, a substrate can be placed for spatial profiling.

an energy distribution that resembles that of the incident gamma-ray beam (bell-shaped distribution plus a linear low-energy tail, see Fig. 5). The electron distribution can be parameterized as a function of the flux and energy distribution of the incident gamma-ray beam (see Figs. 5 and 6), allowing for deconvolution of the electron signal. Once the electron spectrum is measured by a magnetic spectrometer, the spectrum of the incident gamma-ray beam can thus be retrieved with a resolution of the order of the MeV (see Fig. 11). The lead shielding allows for fine selection of the scattered electrons and reduces the off-axis noise induced by photons and particles scattered at a wide angle (see Figs. 9 and 10). In conclusion, the design for a compact gamma-ray spectrometer suited for high-flux gamma-ray beams is presented. The system has an energy resolution of the order of one MeV in an energy window of 3-20 MeV. The performance of the detector is analysed by Monte-Carlo simulations. The system has been tested in recent experimental campaigns (details of the experiment to be published elsewhere [22]) confirming the numerical predictions presented in this manuscript.

ACKNOWLEDGMENTS

The authors are grateful to M. Montgomery for his technical support throughout the project. D.J. Corvan wishes to acknowledge financial support from EPSRC (grant number EP/L013975/1). G. Sarri wishes to acknowledge the financial support from the Leverhlume Trust (grant number ECF-2011-383).

[1] J.Piot B. J.P. Gall L.L. Andersson M. Asai Z. Asfari D. M. Cox F. Dechery O. Dorvaux T. Grahn K. Hauschild G. Henning A. Herzan R.D.Herzberg F. P. Heberger U. Jakobsson P. Jones R. Julin S. Juutinen S. Ketelhut T.L. Khoo M. Leino J. Ljungvall A. Lopez-Martens R. Lozeva P. Nieminen J. Pakarinen P. Papadakis E. Parr P. Peura P. Rahkila S. Rinta-Antila P. Ruotsalainen M. Sandzelius J. Saren C. Scholey D. Seweryniak J. Sorri B. Sulignano Ch. Theisen J. Uusitalo P. T. Greenlees, J. Rubert and M. Venhart. Shell-structure and pairing interaction in superheavy nuclei: Rotational properties of the z=104 nucleus rf. *Physics Review Letters*, 104, 2012.

[2] K.J. Orford. Cosmic gamma-ray bursts. *Nature*, 267, 1977.

[3] P. Biltoft J. Church M.A. Descalle T. Luu D. Manatt G. Mauger E. Norman D. Petersen J. Pruet S. Prussin D. Slaughtera J.M. Hall, S. Asztalos. The nuclear car wash: Neutron interrogation of cargo containers to detect hidden snm. *Nuclear Instruments and Methods in Physics Research Section B: Beam Interactions with Materials and Atoms*, 261, 2007.

[4] A. Bernstein J.A. Church M.A. Descalle T.B. Gosnell J.M. Hall A. Loshak D.R. Manatt G.J. Mauger T.L. Moore E.B. Norman B.A. Pohl J.A. Pruet D.C. Petersen R.S. Walling D.L. Weirup S.G. Prussin M. McDowell

D.R. Slaughter, M.R. Accatino. Preliminary results utilizing high-energy fission product ?-rays to detect fissionable material in cargo. *Nuclear Instruments and Methods in Physics Research Section B: Beam Interactions with Materials and Atoms*, 241, 2005.

[5] P.E. Valk M.N. Maisey D.L. Bailey, D.W. Townsend. *Positron Emission Tomography*. Springer Publishing, 2003.

[6] J.H. Lee C.S. Lee J.S. Lee C.H. Kim S.H. An, H. Seo. Effect of detector parameters on the image quality of compton camera for tc. *Nuclear Instruments and Methods in Physics Research Section A: Accelerators, Spectrometers, Detectors and Associated Equipment*, 571, 2007.

[7] N.H Clinthorne A Czermak W Dulinski J Fuster L Han P Jalocha M Kowal T Kragh C Lacasta G Llosá D Meier M Mikuž E Nygård S.J Park S Roe W.L Rogers B Sowicki P Weilhammer S.J Wilderman K Yoshioka L Zhang A Studen, V Cindro. Effect of detector parameters on the image quality of compton camera for tc. *Nuclear Instruments and Methods in Physics Research Section A: Accelerators, Spectrometers, Detectors and Associated Equipment*, 501, 2003.

[8] A. Baanda W. Przygoda S. Schadmand M.J.A. de Voigt M. Csatlós, J.C.S. Bacelar. Energy response of a novel compact ge+bgo spectrometer for 4-20 MeV gamma - rays. *Nuclear Instruments and Methods in Physics Research Section A: Accelerators, Spectrometers, Detectors and Associated Equipment*, 421, 1999.

[9] G. Pascovici E. Radermacher H.G. Thomas P. von Brentano H. Prade R.M. Lieder M. Wilhelm, J. Eberth. The response of the euroball cluster detector to gamma-ray radiation up to 10 mev. *Nuclear Instruments and Methods in Physics Research Section A: Accelerators, Spectrometers, Detectors and Associated Equipment*, 381, 1996.

[10] M. Vencelj T. Vidmar R.A. Bark E. Gueorguieva F. Komati J.J. Lawrie S.M. Maliage S.M. Mullins S.H.T. Murray T.M. Ramashidzha M. Lipoglavšeka, A. Likar. Measuring high-energy γ-rays with ge clover detectors. *Nuclear Instruments and Methods in Physics Research Section A: Accelerators, Spectrometers, Detectors and Associated Equipment*, 557, 2006.

[11] W. Schumacker et al. to be published. *to be published*, 2014.

[12] A. Fasso A. Ferrari, P.R. Sala and J. Ranft. Fluka: a multi- particle transport code. *CERN-2005-10 , INFN/TC 05/11, SLAC-R-773*, 2005.

[13] S. Roesler P.R. Sala G. Battistoni F. Cerutti E. Gadioli M.V. Garzelli F. Ballarini A. Ottolenghi A. Empl A. Fasso, A. Ferrari and J. Ranft. The physics models of fluka: status and recent developments. *Computing in High Energy and Nuclear Physics 2003 Conference (CHEP2003), La Jolla, CA, USA, March 24?28,*, 2003.

[14] Lifshitz Beresteetskii and Pitaevskii. *L. D. Landau and E. M. Lifshitz The Classical Theory of Fields*, volume 4. Pergamon Press, 4 edition, 1980.

[15] G. Sarri, W. Schumaker, A. Di Piazza, M. Vargas, B. Dromey, M. E. Dieckmann, V. Chvykov, A. Maksimchuk, V. Yanovsky, Z. H. He, B. X. Hou, J. A. Nees, A. G. R. Thomas, C. H. Keitel, M. Zepf, and K. Krushelnick. Table-top laser-based source of femtosecond, collimated, ultrarelativistic positron beams. *Phys. Rev. Lett.*, 110:255002, Jun 2013.

[16] National institute of standards and technology. `http://www.nist.gov/`.

[17] L.G Evans R Starr Y Eisena and J.I Trombka. $cdwo_4$ scintillator as a compact gamma ray spectrometer for planetary lander missions. *Nuclear Instruments and Methods in Physics Research Section A: Accelerators, Spectrometers, Detectors and Associated Equipment*, 490, 2002.

[18] B. A. Remington N. Izumi S. Chen C. Chen G. Kimminau Z. Ali M. J. Haugh B. R. Maddox, H. S. Park and Q. Ma. High-energy x-ray backlighter spectrum measurements using calibrated image plates. *Review of Scientific Instruments*, 82, 2011.

[19] Takashi Sato Ryosuke Kodama Yoneyoshi Kitagawa Teruyoshi Takahashi Toshiji Ikeda Yoshihide Honda Kazuo A. Tanaka, Toshinori Yabuuchi and Shuuichi Okuda. Calibration of imaging plate for high energy electron spectrometer. *Review of Scientific Instruments*, 76, 2005.

[20] Y. Glinec, J. Faure, A. Guemnie-Tafo, V. Malka, H. Monard, J. P. Larbre, V. De Waele, J. L. Marignier, and M. Mostafavi. Absolute calibration for a broad range single shot electron spectrometer. *Review of Scientific Instruments*, 77(10):–, 2006.

[21] Y. Glinec. *Propagation d'une impulsion laser ultra-intense dans un plasma sous-dense Génération de faisceaux d'électrons quasi monoénergétiques et développement d'applications*. PhD dissertation, 2006.

[22] G. Sarri et al. to be published. *to be published*, 2014.